Journal of Geophysical Research: Oceans

RESEARCH ARTICLE
10.1029/2017JC013691

Mercury Inputs to Chinese Marginal Seas: Impact of Industrialization and Development of China

Runsheng Yin[1,2], Zhigang Guo[3], Limin Hu[4], Wenchuan Liu[3], James P. Hurley[5,6], Ryan F. Lepak[5], Tian Lin[7], Xinbin Feng[7], and Xiangdong Li[2]

[1]State Key Laboratory of Ore Deposit Geochemistry, Institute of Geochemistry, Chinese Academy of Sciences, Guiyang, China, [2]Department of Civil and Environmental Engineering, The Hong Kong Polytechnic University, Hung Hom, Kowloon, Hong Kong, [3]Shanghai Key Laboratory of Atmospheric Particle Pollution Prevention, Department of Environmental Science and Engineering, Fudan University, Shanghai, China, [4]Key Laboratory of Marine Sedimentology and Environmental Geology, First Institute of Oceanography, State Oceanic Administration, Qingdao, China, [5]Environmental Chemistry and Technology Program, University of Wisconsin-Madison, Madison, WI, USA, [6]Department of Civil and Environmental Engineering, University of Wisconsin-Madison, Madison, WI, USA, [7]State Key Laboratory of Environmental Geochemistry, Institute of Geochemistry, Chinese Academy of Sciences, Guiyang, China

Key Points:
- The industrialization and hydrologic manipulation can largely alter the inputs of Hg to marginal seas
- Enhanced industrial Hg inputs to the ocean margin, but slightly decreased watershed soil Hg inputs in the last few decades
- Global industrialization has resulted in more inputs of industrial Hg

Supporting Information:
- Supporting Information S1

Correspondence to:
X.D. Li,
cexdli@polyu.edu.hk

Citation:
Yin, R., Guo, Z., Hu, L., Liu, W., Hurley, J. P., Lepak, R. F., et al. (2018). Mercury inputs to Chinese Marginal Seas: Impact of industrialization and development of China. *Journal of Geophysical Research: Oceans*, *123*, 5599–5611. https://doi.org/10.1029/2017JC013691

Received 7 DEC 2017
Accepted 11 MAY 2018
Accepted article online 25 MAY 2018
Published online 15 AUG 2018

Abstract In the past decades, China has experienced substantial economic growth and industrialization. However, the effects of vast development of China on Hg input to the nearby oceans are still unclear. In this study, the influx and isotopic compositions of Hg in four ^{210}Pb-dated sediment cores were examined to investigate changes in Hg deposition to the marginal seas off China over a century. Nearshore cores had higher Hg influxes than offshore cores. Increases of Hg influxes started since the 1950s, which coincides with China's economic development. Dramatic historical changes in Hg isotopic composition were observed in the cores (δ^{202}Hg: −2.01‰ to −0.69‰; Δ^{199}Hg: −0.16‰ to 0.31‰; n = 106). δ^{202}Hg increased from the deep to the surface layers of the cores. The offshore cores mainly showed positive Δ^{199}Hg values, but the pre-1950 samples had more positive Δ^{199}Hg values than the younger samples. The nearshore cores mainly showed negative Δ^{199}Hg values in the pre-1950s samples, but the younger samples showed Δ^{199}Hg values close to zero. A triple-mixing isotope model, used to quantify the contribution of potential Hg inputs (e.g., direct discharge of industrial Hg, soil Hg, and precipitation-derived Hg), showed clear evidence of enhanced industrial Hg inputs to the ocean margin, but slightly decreased watershed soil Hg inputs in the last few decades. The variations of watershed-derived Hg were likely caused by the construction of impoundments in major rivers of China. This study demonstrates that mercury inputs to Chinese marginal seas have been largely altered due to the industrialization and economic development of China.

Plain Language Summary This study demonstrates that mercury inputs to Chinese marginal seas have been largely altered due to industrialization and economic development of China with enhanced industrial Hg inputs to the ocean margin, but slightly decreased watershed soil Hg inputs in the last few decades.

1. Introduction

The atmosphere and ocean play a vital role in the biogeochemical cycling of mercury (Hg), a globally distributed pollutant (Mason et al., 2012). Mercury is released into the environment through both natural and anthropogenic sources, and anthropogenic activities have increased the global cycling of Hg by a factor of 3–5 since the industrial revolution in the 1800s (Amos et al., 2013). Anthropogenic activities not only directly release Hg to the ecosystems, but also release a large amount of Hg into the atmosphere. Atmospheric Hg is mainly (>90%) in gas elemental Hg (GEM) form, which can be globally transported in the atmosphere before deposit to the ecosystems through two pathways: (1) transformation to oxidized Hg (GOM) species which are particle reactive and soluble, and easily deposited through wet/dry deposition; and (2) direct uptake/adsorbed by vegetation and soils followed by oxidation (Demers et al., 2013; Jiskra et al., 2015; Obrist et al., 2017). Mercury enters the ocean primarily through direct atmospheric deposition and watershed runoff of land-based Hg sources (Amos et al., 2014; Sunderland & Mason, 2007; Zhang et al., 2015). Globally, atmospheric Hg deposition (10–29 Mmol yr^{-1}) is in the same magnitude to input by watershed runoff (28 ± 13 Mmol yr^{-1}). However, atmospheric deposition represents the major input of Hg to open oceans

(Sunderland & Mason, 2007), whereas watershed-derived Hg is predominately deposited in margin seas (Amos et al., 2014; Zhang et al., 2015). In the ocean, Hg is subject to scavenging by organic-rich particles, which eventually settle to bottom sediments (Fitzgerald et al., 2007). The concentration of Hg in sediment profiles, coupled with high-resolution age dating (e.g., ^{210}Pb) has been used to evaluate historical changes in Hg deposition (Engstrom et al., 2014).

Mercury has seven stable isotopes (^{196}Hg, ^{198}Hg, ^{199}Hg, ^{200}Hg, ^{201}Hg, ^{202}Hg, and ^{204}Hg), which can exhibit both mass-dependent fractionation (MDF, often reported as Δ^{202}Hg) and mass independent fractionation (MIF, mainly reported as Δ^{199}Hg) during various physical, chemical, and biological processes (Bergquist & Blum, 2007; Blum et al., 2014). Large variations of $>$10‰ in both Δ^{202}Hg and Δ^{199}Hg values have been reported in the Earth's main Hg reservoirs (Blum et al., 2014). Based on the isotopic signature of known Hg sources and Hg isotope fractionation processes, many studies have successfully used binary and triple mixing models to identify and quantify Hg sources in sediments (Donovan et al., 2013; Foucher & Hintelmann, 2009; Lepak et al., 2015; Liu et al., 2011; Yin et al., 2013). However, it needs to be recognized that the use of Hg isotopes for source tracing may lead to ambiguous interpretations, due to the fact of the complexity of Hg isotope fractionation processes as well as the variability of different source signatures. In recent years, mercury isotopes in sediment cores have been utilized to understand Hg deposition history in terrestrial lakes and coastal sites (Balogh et al., 2015; Cooke et al., 2013; Donovan et al., 2013; Gray et al., 2015; Guédron et al., 2016; Ma et al., 2013; Mil-Homens et al., 2013; Sonke et al., 2010; Yin et al., 2016a). In contrast, only few studies reported high-resolution isotopic data on offshore cores of the major ocean, most likely due to low concentrations of Hg and low sedimentation rates (Gehrke et al., 2009; Gleason et al., 2017).

Reconstructing Hg deposition through isotopic compositions is a preferred method for studying Hg in Chinese seas. Of the numerous rivers that flow into China's marginal seas, the Yellow, Yangtze, and Pearl Rivers are the 2nd, 4th, and 17th largest contributors of sediment loads to the global oceans, respectively, resulting in high sedimentation rates in China's marginal seas (Milliman & Meade, 1983). China is now the world's leading producer, user, and emitter of Hg. Rapid economic development in China in the past few decades has released large amounts of Hg to soils, sediments, waters, and atmosphere (Streets et al., 2005). China has also undergone dramatic changes in land use, surface erosion, and dam construction in the upper and middle reaches of many rivers, which in turn affected the watershed input of Hg to the coastal regions. We hypothesize that inputs of Hg to Chinese marginal seas have been significantly changed in the past few decades due to the rapid development of China. To test the hypothesis, this study investigated the concentrations and isotopic compositions of Hg in sediment cores from four major marginal seas off China (Figure 1). Our goals were to evaluate changes in the influx of Hg over the last 100 years, and to use Hg isotopes to quantify the historical changes in different sources of Hg in these coastal environments.

2. Materials and Methods

2.1. Study Area and Sampling

Sediment cores were collected from the four major marginal seas off China (Figure 1), namely the Bohai Sea (BS), Yellow Sea (YS), East China Sea (ECS), and South China Sea (SCS). The BS is a shallow marginal sea with a total area of ~7.7×10^4 km^2, and average depth of 18.7 m. The YS is a semienclosed marginal sea between northeast China and the Korean Peninsula. It has an area of ~3.8×10^5 km^2, and an average depth of 44 m. The ECS is one of the largest marginal seas of the world, covering an area of ~7.7×10^5 km^2, with an average depth of 370 m. The SCS is the second largest marginal sea in the world, which has an area of ~3.5×10^6 km^2, and an average depth of over 2,000 m (Song, 2011). According to the previous studies, the principal sources of sediment along the BS, YS, and ECS are the large rivers, the Yellow River and the Yangtze River. The Yellow River supplies ~10^9 tons of sediment per year, the Yangtze River ~0.48×10^9 tons per year. Other major rivers along Chinese eastern coast (including Liaohe, Luanhe, Haihe, Qiantangjiang, Qujiang, Minjiang, and Hanjiang) together supply not more than 0.06×10^9 tons per year (Li et al., 1991). The largest river in Korea, the Keum River, only supplies 0.006×10^9 tons per year, which is deposited along the Korean coast (Kim & Park, 1992). The Yangtze River is the largest river flowing into the ECS. The discharged sediments are mostly trapped in the Yangtze River Proximal Mud (YRPM) and the Zhejiang-Fujian Coastal Mud (ZFCM), owing to the net effects of the shear forces of the coastal currents (Milliman et al., 1985). In the

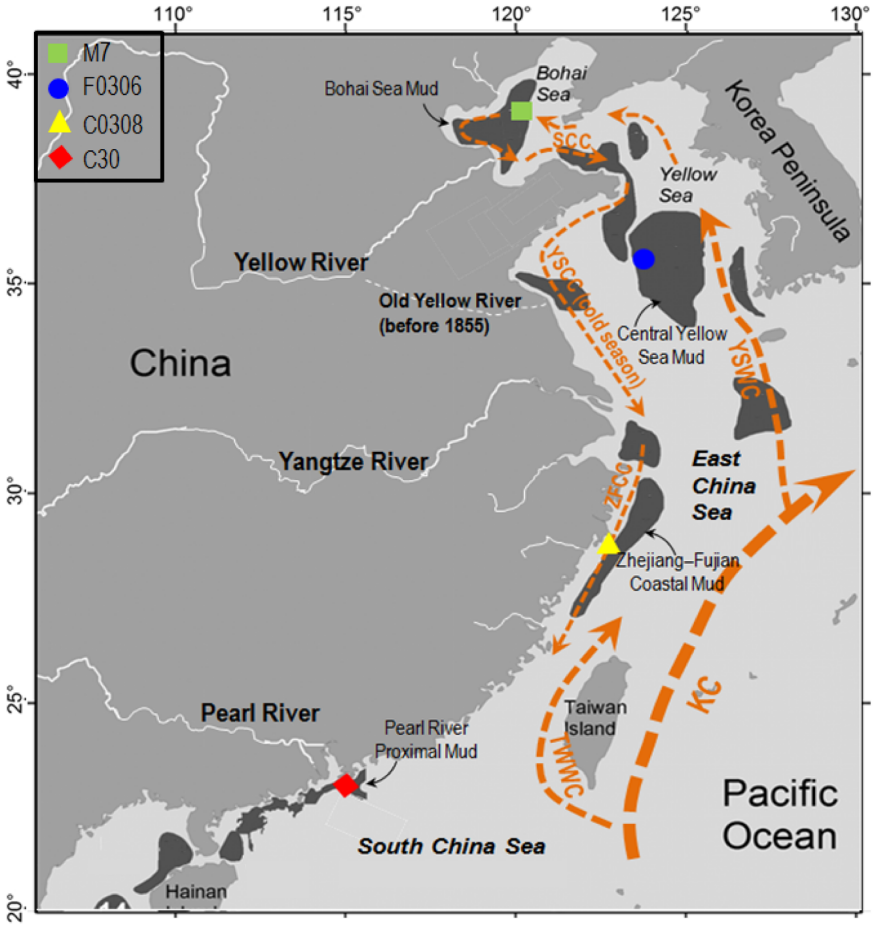

Figure 1. Study area and sampling sites. Continents are light gray colored; mud areas are shown in dark gray colored; currents are shown by orange lines (KC, Kuroshio Current; TWWC, Taiwan Warm Current; YSCC, Yellow Sea Coastal Current; YSWC, Yellow Sea Warm Current; and SCC, Shandong Coast Current).

June–October flood season, the Yangtze discharges ~87% of its mean annual sediments, while the northward Zhejiang-Fujian coastal current (ZFCC) is weak, and the Taiwan Warm Current (TWWC) is strong due to the prevailing southeast monsoon (Guo et al., 2007). This leads to the accumulation of the Yangtze-derived sediments in the subaqueous delta and estuarine system, forming the YRPM. In winter, strong wind-induced waves readily resuspend the newly deposited sediments in the YRPM. The resuspended fine particles are transported southward along the inner shelf by the southward ZFCC driven by the East Asian monsoon and are constrained to the inner shelf of ECS owing to the obstruction of the northward-flowing strong TWWC, thus forming the ZFCM (Guo et al., 2007). Approximately 40% of the Yangtze-derived sediments is deposited in the YRPM, while 32% is believed to be accumulated in the ZFCM (Liu et al., 2007). The Pearl River is the major river flowing into the SCS, discharging ~0.08 $\times$ 10^9 tons of sediments per year (Dai et al., 2009).

In our study, two offshore cores (M7 and F0306) and two nearshore cores (C0803 and C30) were investigated. Core M7 (location: N: 39°53′N; E: 120°46′E; depth: 29 m; length: 53 cm) was collected from the Bohai Sea Mud (BSM) in 2013 using a box corer. Core F0306 (location: 34°59′N, 122°30′E; depth: 65 m; length: 37 cm) was collected from the Yellow Sea Mud (YSM) in 2007 using a box corer. Core C0803 (location: 27°38′N, 121°39′E; depth: 50 m; length: 107 cm) was collected from the ZFCM in the ECS in 2009 using a gravity corer. Samples were sliced at 1 cm intervals. After weighing the total wet sample, about one-eighth of the wet sample was dried in a 110°C oven for 24 h for dry weight measurement. The remainder of the sample was freeze-dried (−20°C) and ground to a fine powder (<74 *m). ^{210}Pb age dating and sediment fluxes of cores F0306,

C0803, and M7 have been previously reported by Li et al. (2016). ^{210}Pb and ^{226}Ra activities were measured using an Ortec HPGe GWL series well-type coaxial low background intrinsic germanium detector, based on the method by Guo et al. (2007). ^{210}Pb was determined by gamma emissions at 46.5 keV, and ^{226}Ra by 295 keV and 352 keV gamma rays emitted by the daughter isotope ^{214}Pb following 3 weeks of storage in sealed containers to allow radioactive equilibration. $^{210}Pb_{ex}$ was calculated by subtracting ^{226}Ra activities from the total ^{210}Pb activities. The relative error for this method was <10%. The constant rate of ^{210}Pb supply (CRS) model was used to calculate the sedimentation rates. The CRS model, which is suitable for a system where the transfer of ^{210}Pb to sediments is very efficient (e.g., large water bodies with long hydraulic retention times) (Appleby et al., 1979), has been widely used by previous studies in Chinese marginal seas (Guo et al., 2007; Ip et al., 2004; Li et al., 2016; Wang et al., 2008). The sediment fluxes were calculated using the outputs of the CRS model and the dry weight test (Ip et al., 2004; Li et al., 2016). Core C30 (location: N: 22°03′N; E: 114°02′E; depth: 18 m; length: 100 cm) from the Pearl River Proximal Mud (PPPM) in SCS was acquired from our previous study, including ^{210}Pb age dating and sedimentation rates (Ip et al., 2004).

2.2. Total Mercury Concentration and Mercury Isotopic Composition Analysis

Total mercury concentrations (THg) of cores C0803, M7, and F0306 were determined using a DMA-80 analyzer (Milestone Inc.) at the Shanghai Key Laboratory of Atmospheric Particle Pollution Prevention, Fudan University, China, following a method described by Liu et al. (2017). Standard reference material (GSS-13, soil) and sample replicates were included for the quality control. Recoveries of THg were 90–110% for GSS-13, and the relative standard deviation of sample duplicates were within 10%. Samples of core C30 was previously digested using aqua regia for THg concentrations determination by the Flow Injection Mercury System (FIMS, Perkin Elmer) using $SnCl_2$ as a reduction reagent (Shi et al., 2010).

Mercury isotopic measurement was performed at the University of Wisconsin-Madison's State Laboratory of Hygiene. About 0.5 g of each sample was digested (95°C, 1 h) in 5 mL of aqua regia (HCl:HNO_3 = 3:1, v:v). According to the THg concentrations measured above, the digest solutions were diluted to contain 0.3–1.0 ng mL^{-1} Hg with acid concentration of <20%. Mercury concentrations and acid matrices of the bracketing Hg standard (NIST SRM 3133) were matched to the sample solutions. Mercury isotope ratios were measured by a Neptune Plus multicollector inductively coupled plasma mass spectrometry (MC-ICP-MS). The MC-ICP-MS was equipped with a gas-liquid phase separator and an Apex-Q desolvation unit (Elemental Scientific Inc., USA) for Hg and thallium (Tl) introduction, respectively. Detailed methods for conducting the MC-ICP-MS analysis were described previously (Yin et al., 2016b). Hg-MDF is expressed in Δ^{202}Hg notation in units of permil (‰) referenced to the NIST-3133 Hg standard (analyzed before and after each sample):

$$\delta^{202}\mathrm{Hg}(‰) = \left[\left(^{202}\mathrm{Hg}/^{198}\mathrm{Hg}_{\mathrm{sample}}\right)/\left(^{202}\mathrm{Hg}/^{198}\mathrm{Hg}_{\mathrm{standard}}\right) - 1\right] \times 1000 \quad (1)$$

Hg-MIF is reported in Δ notation (Δ^{xxx}Hg); it describes the deviation from mass dependency in units of permil (‰). MIF is the difference between the measured δ^{xxx}Hg and the theoretically predicted δ^{xxx}Hg value using the following formula:

$$\Delta^{xxx}\mathrm{Hg} \approx \delta^{xxx}\mathrm{Hg} - \delta^{202}\mathrm{Hg} \times \beta \quad (2)$$

where β is equal to 0.2520 for ^{199}Hg, 0.5024 for ^{200}Hg, and 0.7520 for ^{201}Hg (Blum & Bergquist, 2007).

The THg of the digested samples was also quantified by MC-ICP-MS using ^{202}Hg signals, which were 94–115% of that measured above. Three independent MESS-1 digests were prepared in the same way as the samples, and each digest were diluted to 0.3, 0.5, and 1.0 ng mL^{-1} of Hg in 10% (v/v) aqua regia for isotope measurements. UM-Almadén secondary Hg standard solution containing 0.3, 0.5, and 1.0 ng mL^{-1} of Hg in 10% (v/v) aqua regia was also measured. No statistical differences in Hg isotopic compositions were observed for solutions with different Hg concentrations (Table 1), and the results for UM-Almadén and MESS-1 agreed well with previous reported values (Blum & Bergquist, 2007; Donovan et al., 2013; Yin et al., 2016b). Uncertainties in the data reported in this study reflect the larger values of either the external precision of the replication of the UM-Almadén or the measurement uncertainty of MESS-1.

Table 1
Mercury Isotopic Compositions of UM-Almadén and MESS-1

	Hg (ng/mL)	N	δ^{202}Hg (‰)	2σ (‰0	Δ^{199}Hg (‰)	2σ (‰)	Δ^{200}Hg (‰)	2σ (‰)	Δ^{201}Hg (‰)	2σ (‰)
UM-Almadén	0.3	5	−0.53	0.12	0.02	0.05	0.02	0.04	−0.04	0.05
UM-Almadén	0.5	10	−0.57	0.08	−0.04	0.05	−0.03	0.03	−0.04	0.03
UM-Almadén	1	12	−0.55	0.07	−0.02	0.04	0.01	0.03	−0.03	0.04
MESS-1	0.3	3	−1.95	0.09	−0.02	0.05	−0.02	0.04	−0.04	0.04
MESS-1	0.5	3	−1.96	0.11	0.03	0.04	0.02	0.03	−0.03	0.05
MESS-1	1	3	−1.99	0.07	−0.03	0.04	0.04	0.04	−0.02	0.02

3. Results and Discussion

3.1. Sediment Flux and Mercury Influx

The sediment fluxes varied both among sampling sites and over time (Figure 2). Nearshore C0803 (0.93–0.98 g cm^{-2} yr^{-1}) and C30 (0.38–1.36 g cm^{-2} yr^{-1}) have higher sediment fluxes than offshore cores M7 (0.46–0.60 g cm^{-2} yr^{-1}) and F0306 (0.37–0.52 g cm^{-2} yr^{-1}). Sediment fluxes showed a relatively decreasing trend since the 1980s (Figure 2), which correspond to the effective soil conservation practices and extensive dam and impoundment constructions at the upper stream of Chinese rivers since the 1980s (Wang et al., 2015; Yang et al., 2015). THg concentrations in cores M7, F0306, C0803, and C30 ranged from 16.4 to 33.2, 14.7 to 21.5, 34.5 to 64.7, and 30.4 to 69.3 ng g^{-1}, respectively. At all sites, THg concentrations increased in the last few decades. Nearshore cores C0803 and C30 had higher THg concentrations than offshore cores M7 and F0306 (Figure 2).

Mercury influxes were estimated by THg concentrations multiplied by sediment influx (Ip et al., 2004; Li et al., 2016). As shown in Figure 2, nearshore cores C0803 (33.4–60.7 ng cm^{-2} yr^{-1}) and C30 (24.9–68.5 ng cm^{-2} yr^{-1}) had higher Hg influxes than offshore cores M7 (8.9–15.7 ng cm^{-2} yr^{-1}) and F0306 (5.6–10.1 ng cm^{-2} yr^{-1}). Mercury influxes in cores M7, F0306, and C0803 increased from the deep to the upper layers (Figure 2). The initial increases began in the 1950s, during the Chinese First National Five-Year Plan for economic development. Mercury influxes increased rapidly since the 1980s, which coincided with the launching of China's Economic Reform policy in 1978. Mercury influxes for cores M7, F0306, and C0803 increased by a factor of 1.5–2, whereas lake sediment cores in China (even in Tibet Plateau) and other sites of the world increased by a factor of 3–5 (Balogh et al., 2015; Cooke et al., 2013; Donovan et al., 2013; Ma et al., 2013; Mil-Homens et al., 2013; Gray et al., 2015; Guédron et al., 2016; Sonke et al., 2010; Yang et al., 2010; Yin et al., 2016a). This may be explained by the effective soil conservation practices and extensive dam and impoundment constructions at the higher stream of Chinese rivers in recent decades. China is the world's leading dam builder, and almost all Chinese rivers were intercepted by dams and reservoirs in varying degrees (Vörosmarty et al., 1997). Impoundments and dams cause the suspended particles to settle on short spatial scales, and have resulted in the decrease of sediment load in Chinese rivers (Wang et al., 2015; Yang et al., 2015). The proportion of inflowing sediment retained by a reservoir is averagely 30–40% for global reservoirs (Vörosmarty et al., 1997). Mercury in rivers is predominately in particulate phase, therefore sedimentation in reservoirs would lead to increased Hg deposition in the sediments. A recent study showed that about 40% of the total Hg input can be retained by the reservoirs (Feng et al., 2009). Declined Hg influxes was observed in core C30 in the last three decades, which is likely not only related to the dam constructions, but also the massive, unauthorized sand excavation in the Pearl River at the same period (Wu et al., 2016).

3.2. Mercury Isotopic Composition

The Hg isotopic compositions of our sediment samples were summarized in supporting information Table S1. Large variations in Hg isotopic compositions were observed in cores M7 (δ^{202}Hg: −1.82‰ to −1.05‰; Δ^{199}Hg: 0.07–0.31‰), F0306 (δ^{202}Hg: −1.94‰ to −1.37‰; Δ^{199}Hg: 0.04–0.21‰), C0803 (δ^{202}Hg: −1.89‰ to −0.69‰; Δ^{199}Hg: −0.16‰ to 0.04‰), and C30 (δ^{202}Hg: −2.01‰ to −1.02‰; Δ^{199}Hg: −0.16‰ to 0.08‰) (supporting information Table S1). All of the sediments yielded a Δ^{199}Hg:Δ^{201}Hg ratio of 1.08 ± 0.07 (σ, n = 106), consistent with that reported for aqueous Hg(II) photoreduction (Bergquist & Blum, 2007). Significant MIF of ^{200}Hg was observed in the pre-1980s samples of the core M7 (Δ^{200}Hg: up to 0.20‰), whereas other samples show insignificant MIF of ^{200}Hg. The isotopic composition of the

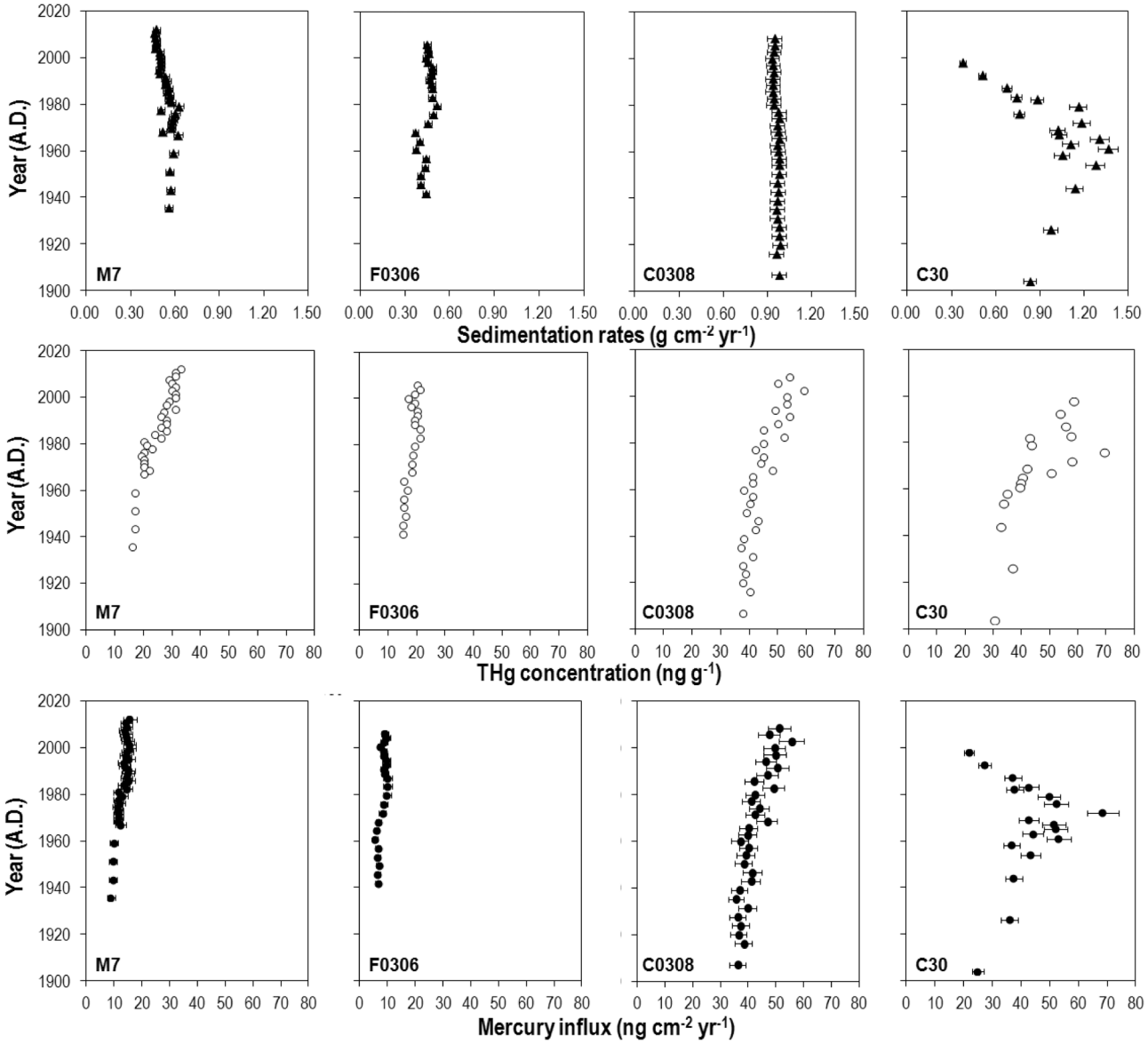

Figure 2. Historical records for sediment flux, THg concentrations, Hg influxes. Cores M7 and F0306 are located at offshore sites, and cores C0803 and C30 are located at nearshore sites. The errors of sediment flux and Hg influx correspond to the relative error (10%) of the ^{210}Pb dating method.

uppermost sample of core C30 (δ^{202}Hg: −1.34‰; Δ^{199}Hg: 0.07‰) was within the range of our previous results about the PRE sediments (δ^{202}Hg: −2.80‰ to −0.68‰; Δ^{199}Hg: −0.15‰ to 0.16‰) (Yin et al., 2015). In previous studies, the variations of Hg isotopes in sediments have been attributed to variations in Hg sources (Balogh et al., 2015; Cooke et al., 2013; Donovan et al., 2013; Gray et al., 2015; Guédron et al., 2016; Ma et al., 2013; Mil-Homens et al., 2013; Sonke et al., 2010; Yin et al., 2016a). In our study, the isotopic compositions of Hg varied over time and among different sampling sites. δ^{202}Hg from all cores increased since the 1950s, and the MIF signals became less pronounced since the 1950s (Figure 3), indicating significant changes in Hg source inventories.

Major inputs of Hg to the ocean include direct atmospheric deposition, and watershed runoff of land-based Hg sources which are further influenced by soil Hg and direct discharge of industrial Hg. By plotting Δ^{202}Hg versus Δ^{199}Hg signals, the three Hg sources are characterized by distinct "δ^{202}Hg-Δ^{199}Hg" signatures (Figure 4). The isotopic signature of industrial Hg can be estimated using Hg polluted sediments with their locations in the vicinity of known industrial sources (Balogh et al., 2015; Bartov et al., 2013; Bonsignore et al., 2015;

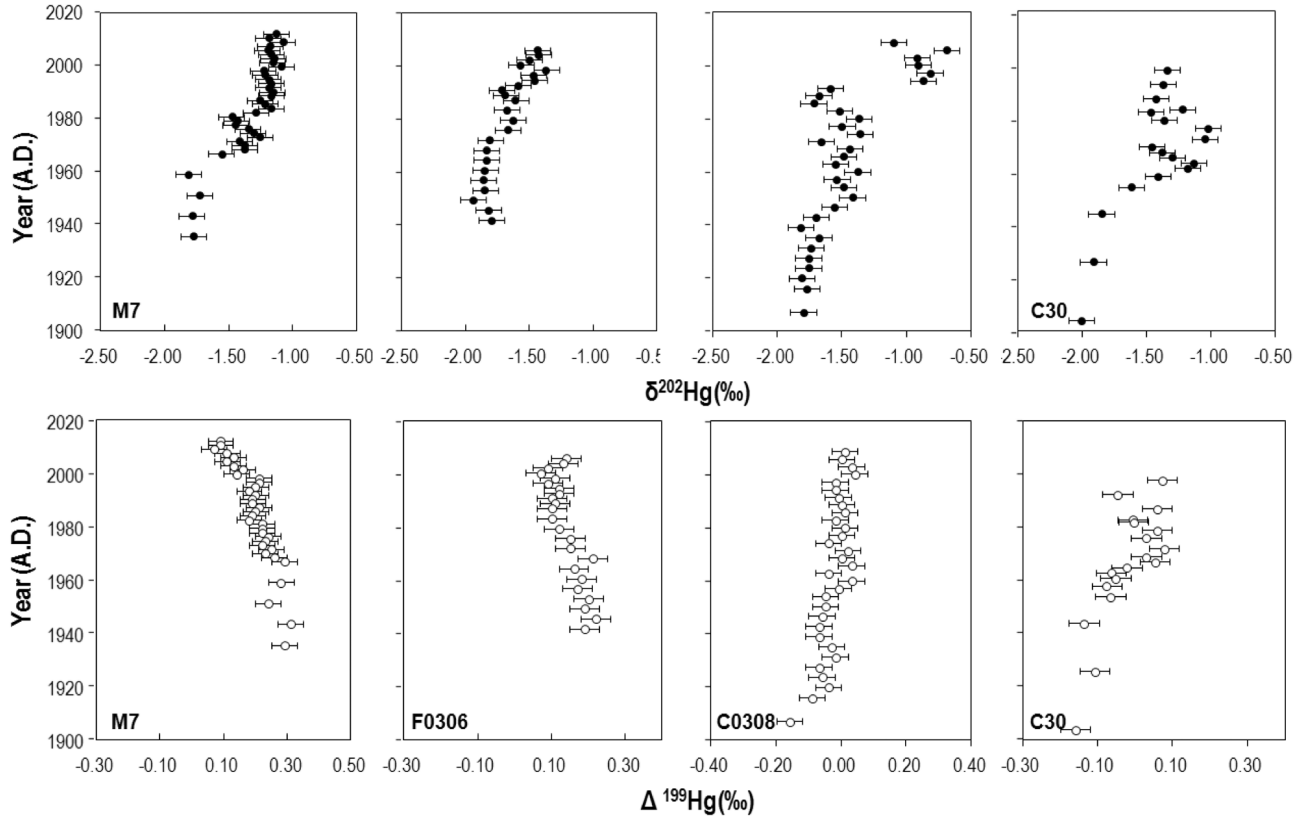

Figure 3. Sediment profiles for δ^{202}Hg and Δ^{199}Hg. Cores M7 and F0306 are located at offshore sites, and cores C0803 and C30 are located at nearshore sites. Errors reflect the larger values of either the external precision of the replication of the UM-Almadén or the measurement uncertainty of MESS-1 (as summarized in Table 1).

Cooke et al., 2013; Donovan et al., 2013; Guédron et al., 2016; Ma et al., 2013; Mil-Homens et al., 2013; Gray et al., 2015; Perrot et al., 2010; Sonke et al., 2010; Wiederhold et al., 2015; Yin et al., 2016a), and hydrothermal ores which are the major source of Hg used in industry (Blum & Bergquist, 2007; Cooke et al., 2013; Feng et al., 2010; Foucher & Hintelmann, 2009; Gray et al., 2013; Smith et al., 2008; Stetson et al., 2009; Wiederhold et al., 2013; Yin et al., 2013, 2016c). Based on the summarization of previous data, we estimated that industrial Hg has mean δ^{202}Hg of -0.53 ± 0.51‰ and mean Δ^{199}Hg of -0.02 ± 0.11‰ (σ, $n = 481$). Mercury is emitted to the atmosphere mainly as elemental Hg(0) form, and is oxidized within the atmosphere to Hg(II), which is the major depositing form of Hg (Mason & Sheu, 2002). While a substantial amount of Hg deposited on the ocean surface is Hg(0), the low solubility of Hg(0), results in a large evasive flux as well. Oxidized Hg(II) species, which are soluble and particle reactive, are more easily deposited through processes such as sorption, complexation, and precipitation. Hg(II) undergoes photoreduction in cloud droplets and surface waters, which imparts negative Δ^{199}Hg values in the produced Hg(0) and positive Δ^{199}Hg values in residue Hg(II) (Bergquist & Blum, 2007; Gratz et al., 2010). Soils with less influences from local industrial Hg contamination, which primarily accumulate Hg(0), have been shown negative Δ^{199}Hg (-0.29 ± 0.12‰, σ, $n = 156$) and lower δ^{202}Hg values (-1.82 ± 0.39‰, σ, $n = 156$) (Biswas et al., 2008; Demers et al., 2013; Jiskra et al., 2017; Wang et al., 2017; Woerndle et al., 2018; Zhang et al., 2013; Zheng et al., 2016). Because soils and vegetation accumulate Hg(0) with lower δ^{202}Hg and negative Δ^{199}Hg values, the Hg(II) species in the atmosphere should be characterized by higher δ^{202}Hg and positive Δ^{199}Hg values. Precipitation, which mainly contains Hg(II) species, is an important pathway of removing Hg(II) from the atmosphere. Precipitation-derived Hg has been shown higher δ^{202}Hg (-1.22 ± 1.08‰, σ, $n = 117$) and positive Δ^{199}Hg (0.38 ± 0.33‰, σ, $n = 117$) (Chen et al., 2012; Demers et al., 2013; Gratz et al., 2010; Sherman et al., 2012, 2015; Wang et al., 2015; Yuan et al., 2018), which may represent the isotopic signature of atmospheric Hg(II).

The isotopic composition of our samples were also plotted in Figure 4a for source identification. Prior to doing this, we expected that all our samples would fall into the triangle of the three potential sources: ①

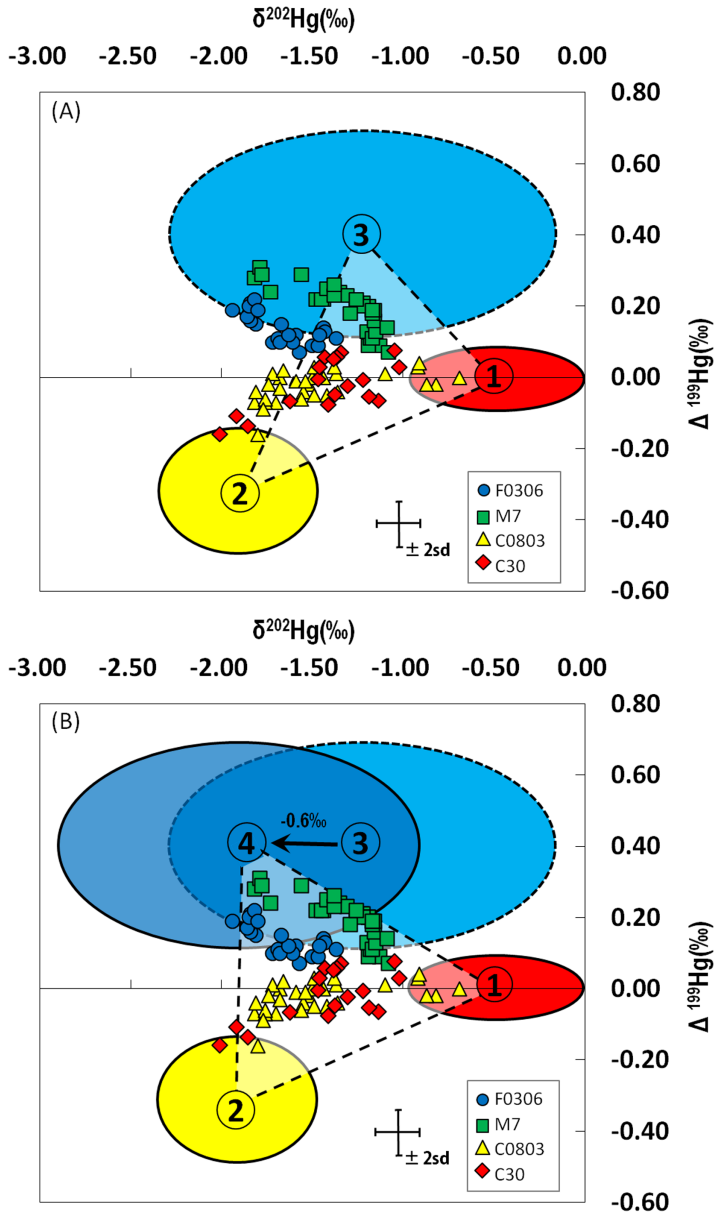

Figure 4. Triple mixing of industrial, watershed, and atmospheric Hg for sediment cores. The solid red circle ① represents industrial Hg (δ^{202}Hg: -0.53 ± 0.51‰; Δ^{199}Hg: -0.02 ± 0.11‰; σ, $n = 481$) (Balogh et al., 2015; Cooke et al., 2013; Donovan et al., 2013; Gray et al., 2015; Guédron et al., 2016; Ma et al., 2013; Mil-Homens et al., 2013; Sonke et al., 2010; Yin et al., 2016a); the solid yellow circle ② represents soils collected from pristine sites (δ^{202}Hg: -1.82 ± 0.39‰; Δ^{199}Hg: -0.29 ± 0.12‰; σ, n = 156) (Biswas et al., 2008; Demers et al., 2013; Jiskra et al., 2017; Wang et al., 2017; Woerndle et al., 2018; Zhang et al., 2013; Zheng et al., 2016); the blue dashed circle ③ represents precipitations (δ^{202}Hg: -1.22 ± 1.08‰; Δ^{199}Hg: 0.38 ± 0.33‰; σ, n = 117) (Chen et al., 2012; Demers et al., 2013; Gratz et al., 2010; Sherman et al., 2012, 2015; Wang et al., 2015; Yuan et al., 2018); and the solid blue circle ④ represents precipitation-derived Hg with a shift of −0.6‰ in δ^{202}Hg.

direct discharge of industrial Hg, ② soil Hg, and ③ precipitation-derived Hg. However, this is not the case in Figure 4a. Many samples fall outside the triangle among ①, ②, and ③ most likely due to isotope fractionation prior to deposition to sediments. For the three potential sources, ① direct discharge of industrial Hg and ② soil Hg should be relatively conservative because it is mainly bound to particles before loading to the sea by rivers. Mercury in major rivers is mainly particulate-bound (~90%), which results in limited isotope fractionation during transport. This enables the use of Hg isotopes to trace the sources of Hg in river and coastal sediments (Foucher & Hintelmann, 2009; Liu et al., 2011; Yin et al., 2013). Unlike soil Hg and industrial Hg, precipitation-derived Hg mainly contains soluble Hg(II) species, which can be absorbed by particles, or reduced and reemitted to the atmosphere. During these processes, the Δ^{202}Hg of precipitation-derived Hg is expected to be altered, because MDF of Hg isotopes have been shown to occur during the adsorption of aqueous Hg(II) by thiol groups (Wiederhold et al., 2010) and goethite (Jiskra et al., 2012), the precipitation of sulfide minerals (Smith et al., 2015), and the microbial and photochemical reduction of aqueous Hg(II) (Bergquist & Blum, 2007; Kritee et al., 2008). Photoreduction of aqueous Hg(II) is the major process causing significant MIF of Hg isotopes in natural samples (Bergquist & Blum, 2007). In the Great Lakes, the transport of precipitation-derived Hg to sediments has been assumed to result in negative shift in δ^{202}Hg values of −0.5‰, but no Δ^{199}Hg shift (Lepak et al., 2015). The shift in δ^{202}Hg values of −0.5‰ can be explained by a combined effect of all MDF processes, such as aqueous Hg(II) adsorption and reduction, and the absence of Δ^{199}Hg shifts can be explained by the limited Hg(II) photoreduction in water column (Lepak et al., 2015). While the global ocean emits a substantial amount of Hg(0) to the atmosphere, the exact magnitude caused by Hg(II) photoreduction is still debated among researchers. It is thought that a substantial amount of Hg emitted to the atmosphere comes from the evasion of previously deposited atmospheric Hg(0). In marginal seas, the photoreduction of Hg(II) may be suppressed by the high levels of halides in seawaters, and by the load of riverine particles. The formation of stable complexes of halides with Hg(II) results in a decrease in the reduction rate (Whalin et al., 2007). Particulate-bound Hg has been demonstrated as the dominant of Hg species in seawaters. The bound of Hg to particles and the high sediment influx in marginal seas could result in rapid burial of Hg into sediments. It is noteworthy that Hg(II) photoreduction mainly occurs only in the surface water. For the major water body (deep waters), the load of riverine particles decreases light penetration, which results in limited Hg(II) photoreduction. Significantly high concentrations of particulate-bound Hg (9.6 ± 3.8 pM) and reactive Hg(II) (4.7 ± 1.4 pM) have been observed in surface waters of the Yellow Sea, China, compared to dissolved Hg(0) species (0.3 ± 0.1 pM) (Ci et al., 2011). Considering that atmospheric deposition contributes Hg(0) to surface water, the dissolved Hg(0) produced by Hg(II) photoreduction may be even lower. In the East China Sea, the dissolved Hg(0) concentrations in the daytime (summer: 62.1 ± 22.1 pg L^{-1}; fall: 51.7 ± 11.6 L^{-1}) were comparable to that in the nighttime (summer: 60.4 ± 17.6 pg L^{-1}; fall: 52.2 ± 21.3 pg L^{-1}) in corresponding season (Wang et al., 2015), which also indicates limited Hg(II) photoreduction. Overall, we hypothesized that Hg(II) photoreduction in marginal seas may be of low magnitude, which may not cause Δ^{199}Hg shift of the

precipitation-derived Hg. In a recent study, insignificant difference in Δ^{199}Hg values with depth were observed in seawater columns of the Canadian Arctic coast (Štrok et al., 2015).

Following the work by Lepak et al. (2015), we also applied a similar negative shift in δ^{202}Hg (−0.6‰) to account the deposition of precipitation-derived Hg to the sediment. The three sources ①, ②, and ④ bracketed all of the sediments that we investigated, enabling sources attribution of Hg in sediments. As shown in Figure 3, the lower δ^{202}Hg and negative Δ^{199}Hg in the pre-1950s samples of nearshore cores C0803 and C30 are interpreted to reflect soil Hg sources. The pre-1950s samples of offshore cores M7 and F0306 have lower δ^{202}Hg and positive Δ^{199}Hg, which suggest the major input of precipitation-derived Hg with additional MDF during adsorption. The increased δ^{202}Hg values and less pronounced MIF signals since the 1950s were consistent with the greater inputs of Hg from industrial sources.

3.3. Quantifying the Different Hg Inputs Using Hg Isotopes

An isotope-based triple mixing model can be invoked to quantify the contributions of direct discharge of industrial Hg, soil Hg, and precipitation-derived Hg in our sediment sediments, where:

$$F_{ind.}+F_{soil}+F_{precip.}=1; \tag{3}$$

$$F_{ind.}*\delta^{202}Hg_{ind.}+F_{soil}*\delta^{202}Hg_{soil}+F_{precip.}*\delta^{202}Hg_{precip.}=\delta^{202}Hg_{spl.}; \tag{4}$$

and

$$F_{ind.}*\Delta^{199}Hg_{ind.}+F_{soil}*\Delta^{199}Hg_{soil}+F_{precip.}*\Delta^{199}Hg_{precip.}=\Delta^{199}Hg_{spl.} \tag{5}$$

In equations 3–5, $F_{ind.}$, F_{soil}, and $F_{precip.}$ represent the fractions of direct discharge of industrial Hg, soil Hg, and precipitation-derived Hg end-members, respectively; $\delta^{202}Hg_{ind.}$, $\delta^{202}Hg_{soil}$, and $\delta^{202}Hg_{precip.}$ represent the δ^{202}Hg of direct discharge of industrial Hg, soil Hg, and precipitation-derived Hg end-members, respectively; $\Delta^{199}Hg_{ind.}$, $\Delta^{199}Hg_{soil}$, and $\Delta^{199}Hg_{precip.}$ represent the Δ^{199}Hg of direct discharge of industrial Hg, soil Hg, and precipitation-derived Hg end-members, respectively; and $\delta^{202}Hg_{spl.}$ and $\Delta^{199}Hg_{spl.}$ represent the δ^{202}Hg and Δ^{199}Hg of a given sample, respectively. This model has been previously used to quantify contribution of discharge of industrial Hg, soil Hg, and precipitation-derived Hg in sediments of the Great Lakes region (Lepak et al., 2015). As shown in Figure 4b, the isotope signatures for ① industrial Hg ($\delta^{202}Hg_{ind.}$: −0.53 ± 0.51‰; $\Delta^{199}Hg_{ind.}$: −0.02 ± 0.11‰), ② soil Hg ($\delta^{202}Hg_{soil}$: −1.82 ± 0.39‰; $\Delta^{199}Hg_{soil}$: −0.29 ± 0.12‰), and ④ precipitation Hg ($\delta^{202}Hg_{precip.}$: −1.22 ± 1.08‰; $\Delta^{199}Hg_{precip.}$: 0.38 ± 0.33‰, with a shift of −0.6‰ in δ^{202}Hg) were used to estimate the fractions of the three end-members for the sediments that we investigated. We used a Monte Carlo error propagation method by the Matlab software to quantify the uncertainties of the model outputs (Guedens et al., 2000), based on the uncertainties of the samples and the uncertainties of the end-members. Mercury influxes of industrial ($Influx_{ind.}$, Hg influx × $F_{ind.}$), watershed ($Influx_{soil}$, Hg influx ×$F_{wat.}$), and atmospheric Hg ($Influx_{precip.}$, Hg influx × $F_{atm.}$) were calculated based on the output of the triple mixing model (Figure 5).

Like many Hg isotope-based binary mixing models (Donovan et al., 2013; Foucher & Hintelmann, 2009; Lepak et al., 2015; Liu et al., 2011; Yin et al., 2013), our model assumes that the isotope signature of a source remain consistent over the study area. The estimated $Influx_{ind.}$, $Influx_{soil}$, and $Influx_{precip.}$ are shown in Figure 5, and we caution our model outputs may have some limitations and uncertainty. $Influx_{ind.}$ of cores M7, F0306, and C0803 started to increase since the middle of last century and accelerated in the 1980s. This correlates with increases in industrial Hg inputs due to economic development in China, which started in the 1950s, and increased rapidly since the 1980s. $Influx_{ind.}$ of core C30 also increased since the 1950s but decreased after the early 1980s. The decrease of $Influx_{ind.}$ in core C30 may be attributed to the decreased loading of contaminated sediments from the Pearl River at the same period (Wu et al., 2016). For cores C0803 and C30 and F0306, significant decreases in $Influx_{soil}$ were observed since the 1980s (Figure 5), which is likely due to the construction of impoundments along major rivers in China during the same period (Wang et al., 2016; Yang et al., 2015). In the past several decades, China has built about 22,000 dams of more than 15 m in height (Vörosmarty et al., 1997), which has resulted in retention of particles and Hg typically transported by rivers (Feng et al., 2009). Unlike other cores, the decrease of $Influx_{soil}$ of core M7 started in the early 1960s, and may be attributed to the major Sanmenxia Hydropower Station built in 1961. From 1961 until the mid-1990s, the Yellow River experienced a decrease in seasonal discharge (Wang et al., 2006), consistent with

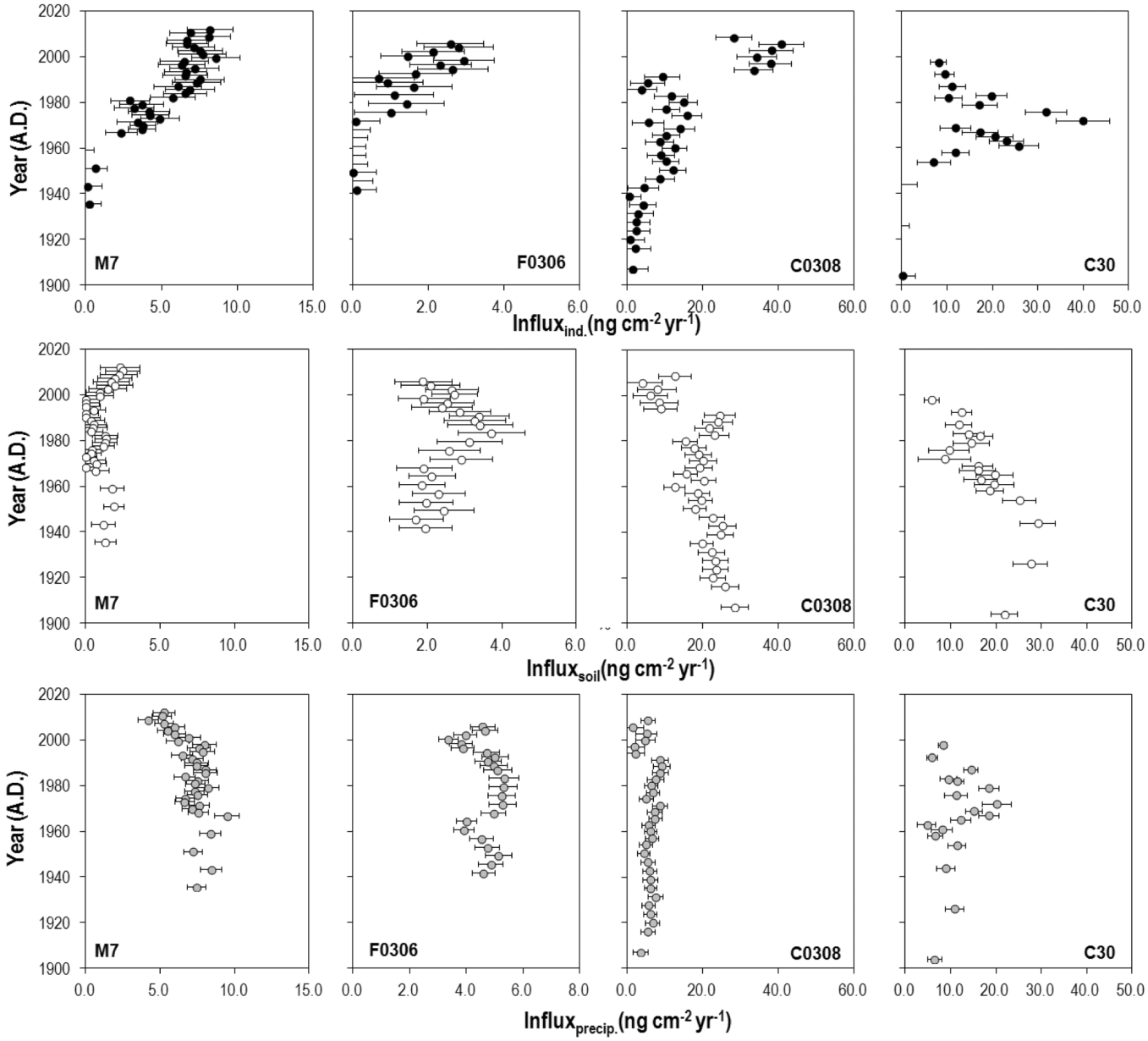

Figure 5. Influxes of industrial (Influx$_{ind.}$), watershed soils (Influx$_{soil}$), and precipitation-derived (Influx$_{precip.}$) Hg in sediment cores. Cores M7 and F0306 are located at offshore sites, and cores C0803 and C30 are located at nearshore sites. The errors were estimated using the error propagation method by the Matlab software, based on the uncertainties of Hg influxes and the uncertainties of the model outputs.

the lowest Influx$_{soil}$ in M7 at the same period. On the Yangtze River, the largest dam in the world (Three Gorges) was built in 1997, and its completion is consistent with the rapid decrease in Influx$_{soil}$ in cores F0306 and C0803 since the late 1990s. Influx$_{precip.}$ values appear to decrease at the four sites in recent decades (Figure 5), which contrasts with an increase Hg emissions in China at the same period. Influx$_{precip.}$ is controlled by annual precipitation rates, and riverine loading of sediment particles which adsorbs precipitation-derived Hg before sedimentation. It is still unclear whether the decreased Influx$_{precip.}$ was caused by decreased rainfall or decreased river sediment load in the recent decades. Therefore, further studies are needed to reveal the key processes involved. Perhaps, the estimated results can explain the positive Δ^{200}Hg in our samples. Among the three input sources (e.g., direct discharge of industrial Hg, soil Hg, and precipitation-derived Hg), only precipitation-derived Hg is characterized by positive Δ^{200}Hg (0.2 ± 0.3‰, σ, n = 104) (Chen et al., 2012; Demers et al., 2013; Gratz et al., 2010; Sherman et al., 2012, 2015; Wang et al.,

2015). $Influx_{precip.}$ accounts for >70% of total Hg input for the pre-1980s samples of core M7, which has pronounced positive Δ^{200}Hg values. For other samples, the positive Δ^{200}Hg signals may be diluted by the industrial and soil Hg sources, because $Influx_{precip.}$ accounts for <50% of total Hg input.

4. Conclusions and Implications

Global industrialization has resulted in more inputs of industrial Hg, resulting in increased atmospheric Hg concentrations about 3- to 5-fold over the preindustrial times. Once emitted, mercury undergoes complicated geochemical cycling in the environment, causing increased Hg levels in terrestrial and marine ecosystems. Mercury isotopes can be fractionated during Hg geochemical cycles, which result in distinguished isotopic signals in different geochemical pools, including the major Hg inputs to the ocean (e.g., direct atmospheric deposition, watershed runoff of soil, and direct industrial discharge). The changes in Hg isotopic signals in sediment cores may reveal relative changes in Hg input sources in history. Using multidimensional Hg isotope tracers (MDF-MIF), our study indicates that the industrialization and economic development of China have largely altered the inputs of Hg to marginal seas. We showed clear evidence of enhanced industrial Hg inputs to the ocean margins in the last few decades, however, hydrologic manipulation in Chinese rivers has also resulted in slightly decreased watershed soil Hg inputs to ocean margins.

Acknowledgments

Runsheng Yin was funded by the Chinese Academy of Sciences through the Hundred Talent Plan. This work was supported by a Seed Collaborative Research Fund (SCRF) grant from the Partner State Key Laboratory of Marine Pollution at City University of Hong Kong, University Facility on Chemical and Environmental Analysis (UCEA) at PolyU, and the Natural Science Foundation of China (41676034 and 41602047). We thank David P. Krabbenhoft from the USGS Wisconsin Mercury Research Lab for providing instrument and lab facilities for this study. Professor S. Bradley Moran and several anonymous reviewers are acknowledged for their constructive comments that have largely improved the quality of this paper. Data and further information of this study are available at PolyU Institutional Research Archive http://ira.lib.polyu.edu.hk/. Runsheng Yin and Zhigang Guo authors contributed equally to this work.

References

Appleby, P. G., Oldfield, F., Thompson, R., Huttunen, P., & Tolonen, K. (1979). ^{210}Pb dating of annually laminated lake sediments from Finland. *Nature*, *280*(5717), 53–55.

Amos, H. M., Jacob, D. J., Kocman, D., Horowitz, H. M., Zhang, Y., Dutkiewicz, S., et al. (2014). Global biogeochemical implications of mercury discharges from rivers and sediment burial. *Environmental Science & Technology*, *48*(16), 9514–9522.

Amos, H. M., Jacob, D. J., Streets, D. G., & Sunderland, E. M. (2013). Legacy impacts of all time anthropogenic emissions on the global mercury cycle. *Global Biogeochemical Cycles*, *27*, 410–421. https://doi.org/10.1002/gbc.20040

Balogh, S. J., Tsui, M. T. K., Blum, J. D., Matsuyama, A., Woerndle, G. E., Yano, S., et al. (2015). Tracking the fate of mercury in the fish and bottom sediments of Minamata Bay, Japan, using stable mercury isotopes. *Environmental Science & Technology*, *49*(9), 5399–5406.

Bartov, G., Deonarine, A., Johnson, T. M., Ruhl, L., Vengosh, A., & Heileen, H. (2013). Environmental impacts of the Tennessee Valley authority Kingston coal ash spill. 1. Source apportionment using mercury stable isotopes. *Environmental Science & Technology*, *47*(4), 2092–2099.

Bonsignore, M., Tamburrino, S., Oliveri, E., Marchetti, A., Durante, C., Berni, A., et al. (2015). Tracing mercury pathways in Augusta Bay (Southern Italy) by total concentration and isotope determination. *Environmental Pollution*, *205*, 178–185.

Bergquist, B. A., & Blum, J. D. (2007). Mass-dependent and-independent fractionation of Hg isotopes by photoreduction in aquatic systems. *Science*, *318*(5849), 417–420.

Biswas, A., Blum, J. D., Bergquist, B. A., Keeler, G. J., & Xie, Z. (2008). Natural mercury isotope variation in coal deposits and organic soils. *Environmental Science & Technology*, *42*(22), 8303–8309.

Blum, J. D., & Bergquist, B. A. (2007). Reporting of variations in the natural isotopic composition of mercury. *Analytical and Bioanalytical Chemistry*, *388*(2), 353–359.

Blum, J. D., Sherman, L. S., & Johnson, M. W. (2014). Mercury isotopes in earth and environmental sciences. *Annual Review of Earth and Planetary Sciences*, *42*, 249–269.

Chen, J. B., Hintelmann, H., Feng, X. B., & Dimock, B. (2012). Unusual fractionation of both odd and even mercury isotopes in precipitation from Peterborough, ON, Canada. *Geochimica et Cosmochimica Acta*, *90*, 33–46.

Ci, Z., Zhang, X., Wang, Z., & Niu, Z. (2011). Phase speciation of mercury (Hg) in coastal water of the Yellow Sea, China. *Marine Chemistry*, *126*(1–4), 250–255.

Cooke, C. A., Hintelmann, H., Ague, J. J., Burger, R., Biester, H., Sachs, J. P., et al. (2013). Use and legacy of mercury in the Andes. *Environmental Science & Technology*, *47*(9), 4181–4188.

Dai, S. B., Yang, S. L., & Li, M. (2009). The sharp decrease in suspended sediment supply from China's rivers to the sea: Anthropogenic and natural causes. *Hydrological Sciences Journal*, *54*(1), 135–146.

Demers, J. D., Blum, J. D., & Zak, D. R. (2013). Mercury isotopes in a forested ecosystem: Implications for air-surface exchange dynamics and the global mercury cycle. *Global Biogeochemical Cycles*, *27*, 222–238. https://doi.org/10.1002/gbc.20021

Donovan, P. M., Blum, J. D., Yee, D., Gehrke, G. E., & Singer, M. B. (2013). An isotopic record of mercury in San Francisco Bay sediment. *Chemical Geology*, *349*, 87–98.

Engstrom, D. R., Fitzgerald, W. F., Cooke, C. A., Lamborg, C. H., Drevnick, P. E., Swain, E. B., et al. (2014). Atmospheric Hg emissions from preindustrial gold and silver extraction in the Americas: A reevaluation from lake-sediment archives. *Environmental Science & Technology*, *48*(12), 6533–6543.

Feng, X., Foucher, D., Hintelmann, H., Yan, H., He, T., & Qiu, G. (2010). Tracing mercury contamination sources in sediments using mercury isotope compositions. *Environmental Science & Technology*, *44*, 3363–3368.

Feng, X., Jiang, H., Qiu, G., Yan, H., Li, G., & Li, Z. (2009). Mercury mass balance study in Wujiangdu and Dongfeng reservoirs, Guizhou, China. *Environmental Pollution*, *157*, 2594–2603.

Fitzgerald, W. F., Lamborg, C. H., & Hammerschmidt, C. R. (2007). Marine biogeochemical cycling of mercury. *Chemical Reviews*, *107*(2), 641–662.

Foucher, D., & Hintelmann, H. (2009). Tracing mercury contamination from the Idrija mining region (Slovenia) to the Gulf of Trieste using Hg isotope ratio measurements. *Environmental Science & Technology*, *43*(1), 33–39.

Gehrke, G. E., Blum, J. D., & Meyers, P. A. (2009). The geochemical behavior and isotopic composition of Hg in a mid-Pleistocene western Mediterranean sapropel. *Geochimica et Cosmochimica Acta*, *73*(6), 1651–1665.

Gleason, J. D., Blum, J. D., Moore, T. C., Polyak, L., Jakobsson, M., Meyers, P. A., et al. (2017). Sources and cycling of mercury in the paleo Arctic Ocean from Hg stable isotope variations in Eocene and Quaternary sediments. *Geochimica et Cosmochimica Acta*, *197*, 245–262.

Gratz, L. E., Keeler, G. J., Blum, J. D., & Sherman, L. S. (2010). Isotopic composition and fractionation of mercury in Great Lakes precipitation and ambient air. *Environmental Science & Technology*, *44*(20), 7764–7770.
Gray, J. E., Pribil, M. J., & Higueras, P. L. (2013). Mercury isotope fractionation during ore retorting in the Almadén mining district, Spain. *Chemical Geology*, *357*, 150–157.
Gray, J. E., Van Metre, P. C., Pribil, M. J., & Horowitz, A. J. (2015). Tracing historical trends of Hg in the Mississippi River using Hg concentrations and Hg isotopic compositions in a lake sediment core, Lake Whittington, Mississippi, USA. *Chemical Geology*, *395*, 80–87.
Guedens, W., Mullens, J., & Poucke, L. V. (2000). Monte Carlo analysis of error propagation in the potentiometric determination of equilibrium constants. *Vaccine*, *9*(12), 914–915.
Guédron, S., Amouroux, D., Sabatier, P., Desplanque, C., Develle, A. L., Barre, J., et al. (2016). A hundred year record of industrial and urban development in French Alps combining Hg accumulation rates and isotope composition in sediment archives from Lake Luitel. *Chemical Geology*, *431*, 10–19.
Guo, Z., Lin, T., Zhang, G., Zheng, M., Zhang, Z., Hao, Y., et al. (2007). The sedimentary fluxes of polycyclic aromatic hydrocarbons in the Yangtze River Estuary coastal sea for the past century. *Science of the Total Environment*, *386*(1), 33–41.
Ip, C. C. M., Li, X. D., Zhang, G., Farmer, J. G., Wai, O. W. H., & Li, Y. S. (2004). Over one hundred years of trace metal fluxes in the sediments of the Pearl River Estuary, South China. *Environmental Pollution*, *132*(1), 157–172.
Jiskra, M., Wiederhold, J. G., Bourdon, B., & Kretzschmar, R. (2012). Solution speciation controls mercury isotope fractionation of Hg(II) sorption to goethite. *Environmental Science & Technology*, *46*(12), 6654–6662.
Jiskra, M., Wiederhold, J. G., Skyllberg, U., Kronberg, R. M., Hajdas, I., & Kretzschmar, R. (2015). Mercury deposition and re-emission pathways in boreal forest soils investigated with Hg isotope signatures. *Environmental Science & Technology*, *49*(12), 7188–7196.
Kim, B. K., & Park, Y. A. (1992). Smectite as a possible source-indicative clay mineral in the Yellow Sea. *Geo-Marine Letters*, *12*(4), 228–231.
Kritee, K., Blum, J. D., & Barkay, T. (2008). Mercury stable isotope fractionation during reduction of Hg (II) by different microbial pathways. *Environmental Science & Technology*, *42*(24), 9171–9177.
Lepak, R. F., Yin, R., Krabbenhoft, D. P., Ogorek, J. M., DeWild, J. F., Holsen, T. M., et al. (2015). Use of stable isotope signatures to determine mercury sources in the Great Lakes. *Environmental Science & Technology Letters*, *2*(12), 335–341.
Li, C. X., Chen, G., Yao, M., & Wang, P. (1991). The influences of suspended load on the sedimentation in the coastal zones and continental shelves of China. *Marine Geology*, *96*(3–4), 341–352.
Li, Y., Lin, T., Hu, L., Feng, J., & Guo, Z. (2016). Time trends of polybrominated diphenyl ethers in East China Seas: Response to the booming of PBDE pollution industry in China. *Environment International*, *92*, 507–514.
Liu, J., Feng, X., Yin, R., Zhu, W., & Li, Z. (2011). Mercury distributions and mercury isotope signatures in sediments of Dongjiang, the Pearl River Delta, China. *Chemical Geology*, *287*(1), 81–89.
Liu, J. P., Xu, K. H., Li, A. C., Milliman, J. D., Velozzi, D. M., Xiao, S. B., et al. (2007). Flux and fate of Yangtze River sediment delivered to the East China Sea. *Geomorphology*, *85*(3), 208–224.
Liu, W., Hu, L., Lin, T., Li, Y., & Guo, Z. (2017). Distribution and mass inventory of mercury in sediment from the Yangtze River estuarine-inner shelf of the East China Sea. *Continental Shelf Research*, *132*, 29–37.
Ma, J., Hintelmann, H., Kirk, J. L., & Muir, D. C. (2013). Mercury concentrations and mercury isotope composition in lake sediment cores from the vicinity of a metal smelting facility in Flin Flon, Manitoba. *Chemical Geology*, *336*, 96–102.
Mason, R. P., Choi, A. L., Fitzgerald, W. F., Hammerschmidt, C. R., Lamborg, C. H., Soerensen, A. L., et al. (2012). Mercury biogeochemical cycling in the ocean and policy implications. *Environmental Research*, *119*, 101–117.
Mason, R. P., & Sheu, G. R. (2002). Role of the ocean in the global mercury cycle. *Global Biogeochemical Cycles*, *16*(4), 1093. https://doi.org/10.1029/2001GB001440
Mil-Homens, M., Blum, J. D., Canário, J., Caetano, M., Costa, A. M., Lebreiro, S. M., et al. (2013). Tracing anthropogenic Hg and Pb input using stable Hg and Pb isotope ratios in sediments of the central Portuguese Margin. *Chemical Geology*, *336*, 62–71.
Milliman, J. D., Huang-Ting, S., Zuo-Sheng, Y., & H. Meade, R. (1985). Transport and deposition of river sediment in the Changjiang estuary and adjacent continental shelf. *Continental Shelf Research*, *4*(1–2), 37–45.
Milliman, J. D., & Meade, R. H. (1983). World-wide delivery of river sediment to the oceans. *The Journal of Geology*, *91*(1), 1–21.
Obrist, D., Agnan, Y., Jiskra, M., Olson, C. L., Colegrove, D. P., Hueber, J., et al. (2017). Tundra uptake of atmospheric elemental mercury drives Arctic mercury pollution. *Nature*, *547*, 201–204.
Perrot, V., Epov, V. N., Pastukhov, M. V., Grebenshchikova, V. I., Zouiten, C., Sonke, J. E., et al. (2010). Tracing sources and bioaccumulation of mercury in fish of Lake Baikal-Angara River using Hg isotopic composition. *Environmental Science & Technology*, *44*, 8030–8037.
Sherman, L. S., Blum, J. D., Dvonch, J. T., Gratz, L. E., & Landis, M. S. (2015). The use of Pb, Sr, and Hg isotopes in Great Lakes precipitation as a tool for pollution source attribution. *Science of the Total Environment*, *502*, 362–374.
Sherman, L. S., Blum, J. D., Keeler, G. J., Demers, J. D., & Dvonch, J. T. (2012). Investigation of local mercury deposition from a coal-fired power plant using mercury isotopes. *Environmental Science & Technology*, *46*(1), 382–390.
Shi, J., Ip, C. C. M., Zhang, G., Jiang, G. B., & Li, X. D. (2010). Mercury profiles in sediments of the Pearl River Estuary and the surrounding coastal area of South China. *Environmental Pollution*, *158*(5), 1974–1979.
Smith, C. N., Kesler, S. E., Blum, J. D., & Rytuba, J. J. (2008). Isotope geochemistry of mercury in source rocks, mineral deposits and spring deposits of the California Coast Ranges, USA. *Earth and Planetary Science Letters*, *269*(3), 399–407.
Smith, R. S., Wiederhold, J. G., & Kretzschmar, R. (2015). Mercury isotope fractionation during precipitation of metacinnabar (β-HgS) and montroydite (HgO). *Environmental Science & Technology*, *49*(7), 4325–4334.
Song, J. (2011). *Biogeochemical processes of biogenic elements in China marginal seas*. Berlin, Germany: Springer Science & Business Media.
Sonke, J. E., Schäfer, J., Chmeleff, J., Audry, S., Blanc, G., & Dupré, B. (2010). Sedimentary mercury stable isotope records of atmospheric and riverine pollution from two major European heavy metal refineries. *Chemical Geology*, *279*(3), 90–100.
Stetson, S. J., Gray, J. E., Wanty, R. B., & Macalady, D. L. (2009). Isotopic variability of mercury in ore, mine-waste calcine, and leachates of mine-waste calcine from areas mined for mercury. *Environmental Science & Technology*, *43*, 7331–7336.
Streets, D. G., Hao, J., Wu, Y., Jiang, J., Chan, M., Tian, H., et al. (2005). Anthropogenic mercury emissions in China. *Atmospheric Environment*, *39*(40), 7789–7806.
Sunderland, E. M., & Mason, R. P. (2007). Human impacts on open ocean mercury concentrations. *Global Biogeochemical Cycles*, *21*, GB4022. https://doi.org/10.1029/2006GB002876
Štrok, M., Baya, P. A., & Hintelmann, H. (2015). The mercury isotope composition of Arctic coastal seawater. *Comptes rendus Geoscience*, *347*(7–8), 368–376.
Vörosmarty, C. J., Sharma, K. P., Fekete, B. M., Copeland, A. H., Holden, J., Marble, J., et al. (1997). The storage and aging of continental runoff in large reservoir systems of the world. *Ambio*, *26*, 269–278.

Wang, C., Ci, Z., Wang, Z., & Zhang, X. (2016). Air-sea exchange of gaseous mercury in the East China Sea. *Environmental Pollution*, *212*, 535–543.
Wang, F., Wang, H., Li, J., Pei, Y., Fan, C., Tian, L., et al. (2008). 2^{10}Pb and ^{137}Cs measurements in the Circum Bohai Sea coastal region: Sedimentation rates and implications. *Frontiers of Earth Science in China*, *2*(3), 276–282.
Wang, H., Yang, Z., Saito, Y., Liu, J. P., & Sun, X. (2006). Interannual and seasonal variation of the Huanghe (Yellow River) water discharge over the past 50 years: Connections to impacts from ENSO events and dams. *Global and Planetary Change*, *50*(3), 212–225.
Wang, S., Fu, B., Piao, S., Lü, Y., Ciais, P., Feng, X., et al. (2015). Reduced sediment transport in the Yellow River due to anthropogenic changes. *Nature Geoscience*, *9*, 38–41.
Wang, X., Luo, J., Yin, R., Yuan, W., Lin, C. J., Sommar, J., et al. (2017). Using mercury isotopes to understand mercury accumulation in the Montane Forest floor of the Eastern Tibetan Plateau. *Environmental Science & Technology*, *51*(2), 801–809.
Wang, Z., Chen, J., Feng, X., Hintelmann, H., Yuan, S., Cai, H., et al. (2015). Mass-dependent and mass-independent fractionation of mercury isotopes in precipitation from Guiyang, SW China. *Comptes Rendus Geoscience*, *347*(7), 358–367.
Whalin, L., Kim, E.-H., & Mason, R. (2007). Factors influencing the oxidation, reduction, methylation and demethylation of mercury species in coastal waters. *Marine Chemistry*, *107*, 278–294.
Wiederhold, J. G., Cramer, C. J., Daniel, K., Infante, I., Bourdon, B., & Kretzschmar, R. (2010). Equilibrium mercury isotope fractionation between dissolved Hg(II) species and thiol-bound Hg. *Environmental Science & Technology*, *44*(11), 4191–4197.
Wiederhold, J. G., Skyllberg, U., Drott, A., Jiskra, M., Jonsson, S., Björn, E., et al. (2015). Mercury isotope signatures in contaminated sediments as a tracer for local industrial pollution sources. *Environmental Science & Technology*, *49*(1), 177–185.
Wiederhold, J. G., Smith, R. S., Siebner, H., Jew, A. D., Brown, G. E. J., Bourdon, B., et al. (2013). Mercury isotope signatures as tracers for Hg cycling at the new Idria Hg mine. *Environmental Science & Technology*, *47*, 6137–6145.
Woerndle, G., Tsui, M. T. K., Sebestyen, S., Blum, J. D., Nie, X., & Kolka, R. K. (2018). New insights on ecosystem mercury cycling revealed by stable isotopes of mercury in water flowing from a headwater peatland catchment. *Environmental Science & Technology*, *52*(4), 1854–1861.
Wu, Z. Y., Saito, Y., Zhao, D. N., Zhou, J. Q., Cao, Z. Y., Li, S. J., et al. (2016). Impact of human activities on subaqueous topographic change in Lingding Bay of the Pearl River estuary, China, during 1955–2013. *Scientific Reports*, *2016*, 6.
Yang, H., Battarbee, R. W., Turner, S. D., Rose, N. L., Derwent, R. G., Wu, G., et al. (2010). Historical reconstruction of mercury pollution across the Tibetan Plateau using lake sediments. *Environmental Science & Technology*, *44*(8), 2918–2924.
Yang, S. L., Xu, K. H., Milliman, J. D., Yang, H. F., & Wu, C. S. (2015). Decline of Yangtze River water and sediment discharge: Impact from natural and anthropogenic changes. *Scientific Reports*, *201*, 5.
Yin, R., Feng, X., Chen, B., Zhang, J., Wang, W., & Li, X. (2015). Identifying the sources and processes of mercury in subtropical estuarine and ocean sediments using Hg isotopic composition. *Environmental Science & Technology*, *49*(3), 1347–1355.
Yin, R., Feng, X., Hurley, J. P., Krabbenhoft, D. P., Lepak, R. F., Zhang, Q., et al. (2016c). Mercury isotopes as proxies to identify sources and environmental impacts of mercury in sphalerites. *Scientific Reports*, *5*, 18686.
Yin, R., Feng, X., Wang, J., Li, P., Liu, J., Zhang, Y., et al. (2013). Mercury speciation and mercury isotope fractionation during ore roasting process and their implication to source identification of downstream sediment in the Wanshan mercury mining area, SW China. *Chemical Geology*, *336*, 72–79.
Yin, R., Krabbenhoft, D. P., Bergquist, B. A., Zheng, W., Lepak, R. F., & Hurley, J. P. (2016b). Effects of mercury and thallium concentrations on high precision determination of mercury isotopic composition by Neptune Plus multiple collector inductively coupled plasma mass spectrometry. *Journal of Analytical Atomic Spectrometry*, *31*(10), 2060–2068.
Yin, R., Lepak, R. F., Krabbenhoft, D. P., & Hurley, J. P. (2016a). Sedimentary records of mercury stable isotopes in Lake Michigan. *Elementa: Science of the Anthropocene*, *4*, 86.
Yuan, S., Chen, J., Cai, H., Yuan, W., Wang, Z., Huang, Q., et al. (2018). Sequential samples reveal significant variation of mercury isotope ratios during single rainfall events. *Science of the Total Environment*, *624*, 133–144.
Zhang, H., Yin, R., Feng, X., Sommar, J., Anderson, C. W. N., Sapkota, A., et al. (2013). Atmospheric mercury inputs in montane soils increase with elevation: Evidence from mercury isotope signatures. *Scientific Reports*, *3*, 3322.
Zhang, Y., Jacob, D. J., Dutkiewicz, S., Amos, H. M., Long, M. S., & Sunderland, E. M. (2015). Biogeochemical drivers of the fate of riverine mercury discharged to the global and Arctic oceans. *Global Biogeochemical Cycles*, *29*, 854–864. https://doi.org/10.1002/2015GB005124
Zheng, W., Obrist, D., Weis, D., & Bergquist, B. A. (2016). Mercury isotope compositions across North American forests. *Global Biogeochemical Cycles*, *30*, 1475–1492. https://doi.org/10.1002/2015GB005323